Constraining the interactions in the dark sector with cosmological data

Adrià Gómez-Valent[1,*], Valeria Pettorino[2] and Luca Amendola[1]

[1] *Institut für Theoretische Physik, Ruprecht-Karls-Universität Heidelberg, Philosophenweg 16, D-69120 Heidelberg, Germany*
E-mail: gomez-valent@thphys.uni-heidelberg.de

[2] *AIM, CEA, CNRS, Université Paris-Saclay, Université Paris Diderot, Sorbonne Paris Cité F-91191 Gif-sur-Yvette, France*

We provide constraints on coupled dark energy (CDE) cosmology with Peebles-Ratra (PR) potential, $V(\phi) = V_0\phi^{-\alpha}$, and constant coupling strength β. This modified gravity scenario introduces a fifth force between dark matter particles, mediated by a scalar field that plays the role of dark energy. The mass of the dark matter particles does not remain constant, but changes with time as a function of the scalar field. Here we assess the ability of the model to describe updated cosmological data sets that include the *Planck* 2018 cosmic microwave background (CMB) temperature, polarization and lensing, baryon acoustic oscillations, the Pantheon compilation of supernovae of Type Ia, data on $H(z)$ from cosmic chronometers, and redshift-space distortions. We also study the impact of the local measurement of H_0 from SH0ES and the strong-lensing time delay data from the H0LICOW collaboration on β. We find a peak corresponding to a coupling $\beta > 0$ and to a potential parameter $\alpha > 0$, more or less evident depending on the data set combination. We show separately the impact of each data set and remark that it is especially CMB lensing the one data set that shifts the peak the most towards ΛCDM. When a model selection criterion based on the full Bayesian evidence is applied, however, ΛCDM is still preferred in all cases, due to the additional parameters introduced in the CDE model. The model is not able to loosen significantly the H_0 tension. This contribution to the proceedings of the DM1 parallel session of the 16th Marcel Grossmann virtual Conference: "Interacting dark matter" is based on the paper 2004.00610.[1]

Keywords: Cosmology: observations; Cosmology: theory; cosmological parameters; dark energy; dark matter.

1. Introduction

Important observational hints in favor of the positive acceleration of the Universe appeared already more than twenty years ago, thanks to the detection of standardizable high-redshift supernovae of Type Ia (SNIa) and the measurement of their light-curves and redshifts.[2,3] Since then, many other probes have contributed to increase the evidence in favor of the late-time accelerated phase. They range e.g. from the detection of the baryon acoustic peak in the two-point correlation function of matter density fluctuations[4,5] to the very accurate measurement of the cosmic microwave background (CMB) temperature anisotropies by WMAP[6] and *Planck*.[7–9]

*Speaker. E-mail: gomez-valent@thphys.uni-heidelberg.de

At the phenomenological level, the easiest explanation for such acceleration is given by the presence of a very tiny cosmological constant in Einstein's field equations, with an associated energy density which is orders of magnitude lower than the quantum field theoretical estimates made for the vacuum energy density. Protecting such low value from radiative corrections is extremely difficult and constitutes the core of the so-called "old" cosmological constant problem, cf. e.g.[10–12] In addition, explaining why the current value of this energy density is of the same order of magnitude as the matter energy density, the so-called "coincidence problem", is considered by part of the cosmological community as another problem that needs to be addressed. The cosmological constant is a pivotal ingredient of the standard cosmological model, also known as ΛCDM or concordance model (cf. e.g. the reviews[13,14]), which can explain most of the cosmological observations with high proficiency. Nevertheless, the aforementioned theoretical conundrums, together with few persistent tensions in some relevant parameters of the model as the Hubble parameter H_0[9,15] and the root-mean-square (*rms*) of mass fluctuations at scales of $8h^{-1}$ Mpc,[16] σ_8 (or $S_8 = \sigma_8(\Omega_m^{(0)}/0.3)^{0.5}$ [a17]), with h being the reduced Hubble parameter, motivate theoretical cosmologists to look for alternative scenarios in which these problems can be solved or, at least, alleviated, see[18,19] and references therein. Wherever the solution comes from, i.e. a departure from General Relativity or some sort of new field describing dark energy (DE), it must mimic very well the behavior of a cosmological constant at low redshifts, meaning that the corresponding effective equation of state (EoS) parameter must be very close to -1, and that the new component must not be able to cluster efficiently at low scales.

In this paper we consider a scenario in which dark matter (DM) particles interact via a force mediated by a scalar field, which in turn drives cosmic acceleration. This scenario is referred to as *coupled dark energy* (CDE). It was originally proposed as a means of alleviating the coincidence problem,[20,21] considering not only a potential energy density for quintessence to generate its dynamics, but also allowing an interaction with other sectors of the theory. These interactions extended the original quintessence models.[22–25] They cannot be ruled out *a priori* and, hence, they must be duly constrained by experiments and observations.

Some works already set constraints on this model, but using older cosmological data sets, for instance CMB data from the WMAP satellite and the South Pole Telescope,[26] or considering past (2013, 2015) releases of *Planck* CMB data in combination with other data sets, as e.g. from baryon acoustic oscillations (BAO) and SNIa,[27,28] Intriguingly, these works detected a likelihood peak at a non-vanishing value of the coupling constant. One of our main goals is then to critically revisit and update these results in the light of the recent strengthening of the H_0 tension and of the rich amount of currently available data at our disposal, in particular the *Planck* 2018 CMB temperature, polarization and lensing data, but also other new cosmological data, for instance Refs.[29,30]. For constraints on other models with DM-DE

[a]The superscripts (0) will denote from now on quantities evaluated at present, i.e. at $a = 1$.

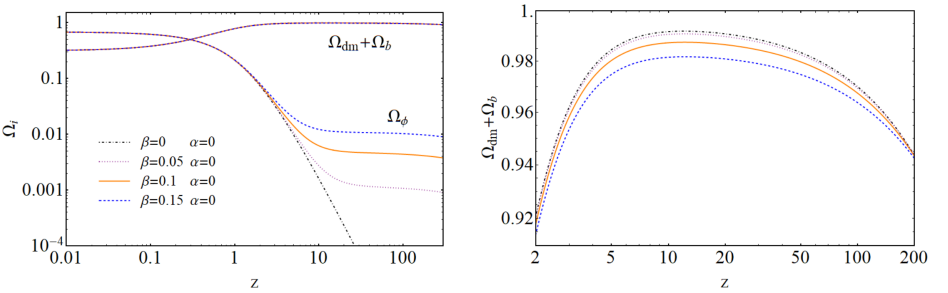

Fig. 1. *Left plot:* Normalized densities $\Omega_{dm}(z)+\Omega_b(z)$ and $\Omega_\phi(z)$ for four alternative values of β and considering a constant potential. The other parameters (including the current energy densities) have been set to the best-fit ΛCDM values from the TTTEEE+lowE *Planck* 2018 analysis.[9] *Right plot:* Here we zoom in the range $z=[2,200]$ of the $\Omega_{dm}+\Omega_b$ curves in order to better visualize their evolution during the matter-dominated epoch, when the system is near the ϕMDE fixed point. See the text for details.

interactions see e.g.,[31–44] and when the interaction is motivated in the context of the running vacuum models.[40,41,45–48]

2. Coupled dark energy

We consider a CDE scenario, as studied in,[21,49,50] to which we refer for a detailed description. We here briefly recall the main equations. This CDE model is formulated in the so-called Einstein or observational frame.[51] Apart from the Standard Model of Particle Physics and a potential extension accounting for the origin of the neutrino masses, we consider a dark sector described by the following Lagrangian density:

$$\mathcal{L}_{\rm dark}=-\partial_\mu\phi\partial^\mu\phi-V(\phi)-m(\phi)\bar{\psi}\psi+\mathcal{L}_{\rm kin}[\psi]\,, \tag{1}$$

where ϕ is the scalar field that plays the role of DE, with potential $V(\phi)$, and ψ is the DM field, considered here to be of fermionic nature, just for illustrative purposes. The DM particles interact with the DE due to the ϕ-dependent mass term appearing in (1). Such interaction introduces a fifth force that alters the trajectory in spacetime of the DM with respect to the one found in the uncoupled case. As we do not couple ϕ to the standard model sector we avoid the stringent local (Solar System) constraints on the violation of the weak equivalence principle,[52] and also on screened fifth forces that couple ϕ to non-dark matter, e.g. from Casimir experiments,[53] precision measurements of the electron magnetic moment,[54] or measurements of the Eötvös parameter.[55] They have no impact on the CDE model under study.

The variation of the total action with respect to the metric leads as usual to Einstein's equations, and the covariant energy of the joint system DM-DE is conserved. Hence, $\nabla^\mu T^\phi_{\mu\nu}=+Q_\nu$ and $\nabla^\mu T^{dm}_{\mu\nu}=-Q_\nu$, with Q_ν defined as

$$Q_\nu=\beta\kappa T^{dm}\nabla_\nu\phi\,, \tag{2}$$

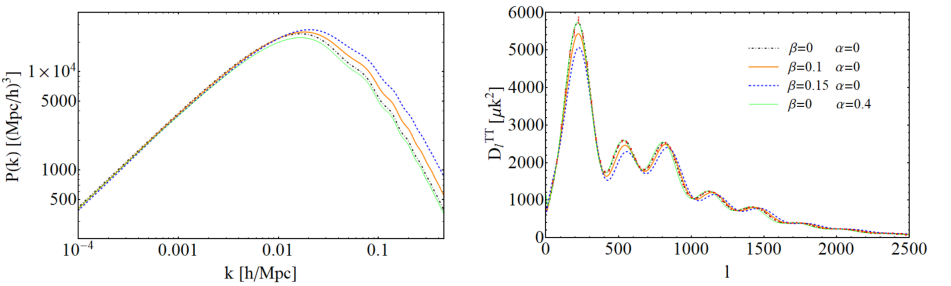

Fig. 2. Theoretical curves of the current matter power spectrum (left plot) and CMB temperature anisotropies (right plot) for the ΛCDM, two CDE models with $\beta = 0.1, 0.15$ and flat potential, and also for the uncoupled Peebles-Ratra model with $\alpha = 0.4$. We set the other parameters as in Fig. 1. In the right plot we also include the observational data from[9] (in red). These figures show: (i) the enhancement of the growth of matter perturbations caused by $\beta > 0$, and the opposite effect produced by $\alpha > 0$; and (ii) the shift to larger multipoles and the amplitude suppression of the acoustic peaks induced by increasing values of β. See the text for further details.

where $\kappa = \sqrt{8\pi G}$, T^{dm} is the trace of the DM energy-momentum tensor, and β controls the strength of the interaction and is in general a function of ϕ. If set to zero, we recover the equations of uncoupled quintessence. In this work we consider β to be a positive constant.

We assume that the Universe is spatially flat, as supported by CMB information from *Planck* 2018 when combined with BAO[9] and/or SNIa,[56] with the curvature parameter $\Omega_K^{(0)}$ constrained to be lower than $\sim 2\%$ at 68% c.l. in ΛCDM. Thus, we can make use of the Friedmann-Lemaître-Robertson-Walker metric, which at the background level reads $ds^2 = a^2(\tau)\left[-d\tau^2 + \delta_{ij}dx^i dx^j\right]$, with a being the scale factor, τ the conformal time, and x^i for $i = 1, 2, 3$ the spatial comoving coordinates. In addition, we treat DM as a pressureless perfect fluid, so the conservation equations for DE and DM can be written, respectively,

$$\beta\kappa a^2 \rho_{dm} = \phi'' + 2\mathcal{H}\phi' + a^2 \frac{\partial V}{\partial \phi}\,, \tag{3}$$

$$\rho'_{dm} + 3\mathcal{H}\rho_{dm} = -\beta\kappa\rho_{dm}\phi'\,, \tag{4}$$

with ρ_{dm} the DM energy density, $\mathcal{H} = a'/a$, and the primes denoting derivatives *w.r.t.* the conformal time. All the functions entering these equations are background quantities. If we assume the conservation of the number density of DM particles then their mass evolves as $m(\phi) = m^{(0)} e^{\beta\kappa(\phi^{(0)} - \phi)}$.

A feature of the model is that for $\beta^2 < 3/2$ it has an unstable (saddle) fixed point at $(\Omega_{dm}, \Omega_\phi) = (1 - 2\beta^2/3, 2\beta^2/3)$, where $\Omega_i = \rho_i/\rho_c$, with ρ_c the critical energy density. This fixed point (dubbed ϕMDE in[21]) cannot be reached exactly, since there is also a non-null fraction of baryons, but the system can be quite close to it, since the DM energy density is much larger than the baryonic one (cf. Fig. 1). During this phase the effective EoS parameter, i.e. the ratio of the total pressure

and the critical energy density in the Universe, is given by $w_{\rm eff} = \Omega_\phi$, and hence the deceleration parameter reads $q = \frac{1}{2}(1+3\,w_{\rm eff}) = \frac{1}{2}+\beta^2$. Thus, the coupling between DM and DE makes the Universe more decelerated with respect to the uncoupled quintessence case during the matter-dominated epoch (MDE). This fact together with the fifth force that enters now as a new source term in the Poisson equation help matter inhomogeneities to grow faster for larger values of β. We also remark that for fixed values of the present energy densities, matter becomes dominant over radiation earlier in time when $\beta > 0$, with respect to the uncoupled case. In the CDE scenario, the equation for the DM density contrast $\delta_{dm} = \delta\rho_{dm}/\rho_{dm}$ at deep subhorizon scales ($k \gg \mathcal{H}$) and when non-linear processes are unimportant, reads,

$$\delta''_{dm} + (\mathcal{H} - \ \beta\kappa\phi')\delta'_{dm} - 4\pi G a^2[\rho_b\delta_b + \rho_{dm}\delta_{dm}(1+2\beta^2)] = 0\,. \tag{5}$$

If we neglect the contribution of baryons, $\delta_m(a) \sim a^{1+2\beta^2}$. Hence, larger values of β enhance the matter power spectrum (see the left plot of Fig. 2) and leave an imprint on the CMB temperature anisotropies. First, the integrated Sachs-Wolfe effect[57] is enhanced during the MDE earlier than in the uncoupled scenario, in which such effect is only relevant after matter-domination; second, the coupling affects lensing of CMB by large scale structure; the interaction also shifts the position of the acoustic peaks to larger multipoles due to the decrease of the sound horizon at the baryon-drag epoch, which is caused by the increase of the mass of the DM particles. Finally, the amplitude is suppressed, because of the decrease of ρ_b/ρ_{dm} at recombination. These two effects explain why the coupling strength is degenerate with the Hubble parameter today,[27] whose value is related to the position and overall amplitude of the first peak. These and other aspects of the structure formation were already discussed in.[50,58–60] See therein for further details, and also the plots in Fig. 2.

The quintessence potential only rules the dynamics of ϕ in the late-time universe, after the MDE, when the interaction term appearing in the *l.h.s.* of (3) becomes subdominant. It helps to slow down structure formation processes *w.r.t.* the flat-potential scenario (for a fixed value of the current DE density). Hence, it can compensate in lesser or greater extent (depending on its steepness) the enhancement of power generated by the fifth force during the MDE (cf. the left plot of Fig. 2 and its caption).

We employ the Peebles-Ratra (PR) potential,[24,25]

$$V(\phi) = V_0\phi^{-\alpha}\,, \tag{6}$$

with V_0 and $\alpha > 0$ being constants, and the former having dimensions of mass$^{4+\alpha}$ in natural units, since ϕ has dimensions of mass. We want to update the constraints on the parameters of the CDE model with PR potential that were obtained in some past works using older CMB data, from WMAP and/or past releases of *Planck* (cf.[26–28,61]), so it is natural to stick to (6) here. Also because it has proved to be capable of improving the description of some cosmological data sets with respect to the ΛCDM model in the non-interactive case.[62–64]

The CDE model we are considering (i.e. CDE with PR potential) has three nested models, namely the ΛCDM, the PR model, and the CDE model with flat potential. They are obtained from the full CDE model with (6) in the limits $(\alpha, \beta) \to (0, 0)$, $\beta \to 0$ and $\alpha \to 0$, respectively. For constraints on these scenarios cf. appendix B of Ref.[1].

For recent studies on CDE with an exponential potential, see[31,33,34,43] and appendix C of Ref.[1]. The results are very similar to the ones obtained with the PR potential.

3. Methodology and data

We have implemented the CDE model described in Sec. 2 in our own modified version of the Einstein-Boltzmann system solver `CLASS`.[65] The Bayesian exploration of the parameter space of the model in the light of the various data sets has been carried out with the Monte Carlo sampler `Montepython`.[66] We have also used the `Python` package `GetDist`[67] to process the chains and obtain the mean values and uncertainties of the parameters reported in Table 1, as well as the contours of Figs. 3-4. Finally, we have computed the full Bayesian evidences for all the models and under the various data sets, by processing the corresponding Markov chains with the code `MCEvidence`.[68] This has allowed us to carry out a rigorous model comparison analysis, which we present in Sec. 4.

Our data set is very similar to the one used by the *Planck* collaboration in their 2018 analysis of the ΛCDM and minimal extensions of it.[9] There are some differences, though, e.g. we analyze here the effect of cosmic chronometers and the H0LICOW data, something that was not done there. We refer the reader to Sec. 3 and reference[9] for details.

This is the list of individual data sets that we employ in this work to constrain the CDE model presented in Sec. 2:

- CMB: The main results of this paper are derived making use of the full TTTEEE+lowE CMB likelihood from *Planck* 2018.[9] We also study what is the impact of also including the CMB lensing likelihood.[69]
- BAO: We use the data points reported in[30,70–75]
- SNIa: We consider 6 effective points on the Hubble rate, i.e. $E(z) \equiv H(z)/H_0$, and the associated covariance matrix. They compress the information of 1048 SNIa contained in the Pantheon compilation[76] and the 15 SNIa at $z > 1$ from the Hubble Space Telescope Multi-Cycle Treasury programs.[77]
- Cosmic chronometers (CCH): We have employed the 31 data points on $H(z_i)$ at various redshifts provided in.[78–85] More concretely, we make use of the *processed* sample provided in Table 2 of,[86] which is more conservative, since it introduces corrections accounting for the systematic errors mentioned above.

Table 1. Constraints obtained using the data set combinations described in Sec. 3 on the following parameters of the CDE model: the reduced DM and baryon energy densities, $\Omega_{dm}^{(0)}h^2$ and $\Omega_b^{(0)}h^2$; the reionization optical depth, τ; the Hubble parameter, H_0 (in units of km/s/Mpc); the power of the primordial power spectrum, n_s; the current amplitude of mass fluctuations at $8h^{-1}$ Mpc, σ_8; the coupling strength β; and the power of the PR potential (6). We provide the mean values and 68% confidence intervals for each of them. We also show the differences *w.r.t.* the ΛCDM of the minimum values of the χ^2-function, and the natural logarithm of the Bayes ratio $B_{\rm CDE,\Lambda}$, as defined in (9)-(10). The (small) negative values of $\chi^2_{min.\rm CDE} - \chi^2_{min,\Lambda}$ tell us that CDE is able to fit slightly better the data than the ΛCDM; if we use as an alternative estimator the Bayes factor, we find negative values of $\ln(B_{\rm CDE,\Lambda})$, indicating a preference for the ΛCDM model. See Sec. 4 for a thorough discussion.

Parameter/Info. criteria	P18	P18+BSC
$\Omega_{dm}^{(0)}h^2$	$0.1207^{+0.0014}_{-0.0013}$	0.1192 ± 0.0008
$\Omega_b^{(0)}h^2$	0.02237 ± 0.00015	$0.02242^{+0.00010}_{-0.00015}$
τ	0.0538 ± 0.0070	$0.0532^{+0.0075}_{-0.0087}$
H_0	$67.74^{+0.57}_{-0.66}$	68.41 ± 0.38
n_s	$0.9654^{+0.0035}_{-0.0042}$	0.9690 ± 0.0038
σ_8	0.8164 ± 0.0076	0.8104 ± 0.0076
α	< 0.50	0.52 ± 0.17
β	$0.0158^{+0.0067}_{-0.0120}$	$0.0206^{+0.0070}_{-0.0095}$
$\chi^2_{min,\rm CDE} - \chi^2_{min,\Lambda}$	-0.02	-0.28
$\ln B_{\rm CDE,\Lambda}$	-8.05	-9.95
Parameter	P18+SH0ES+H0LICOW	P18+BSC+RSD
$\Omega_{dm}^{(0)}h^2$	$0.1172^{+0.0012}_{-0.0014}$	0.1187 ± 0.0008
$\Omega_b^{(0)}h^2$	$0.02262^{+0.00016}_{-0.00014}$	$0.02253^{+0.00010}_{-0.00012}$
τ	0.0594 ± 0.0074	0.0501 ± 0.0052
H_0	$69.43^{+0.72}_{-0.53}$	$68.64^{+0.30}_{-0.38}$
n_s	0.9731 ± 0.0042	$0.9701^{+0.0029}_{-0.0033}$
σ_8	$0.8121^{+0.0065}_{-0.0080}$	0.8048 ± 0.0052
α	1.32 ± 0.18	$0.67^{+0.11}_{-0.16}$
β	$0.0294^{+0.0120}_{-0.0076}$	$0.0151^{+0.0073}_{-0.0083}$
$\chi^2_{min,\rm CDE} - \chi^2_{min,\Lambda}$	-0.58	-1.56
$\ln B_{\rm CDE,\Lambda}$	-7.57	-8.33
Parameter	P18lens+BSC+RSD	P18+BSC+SH0ES+H0LICOW
$\Omega_{dm}^{(0)}h^2$	0.1191 ± 0.0007	0.1185 ± 0.0008
$\Omega_b^{(0)}h^2$	$0.02253^{+0.00013}_{-0.00011}$	$0.02253^{+0.00011}_{-0.00013}$
τ	$0.0525^{+0.0052}_{-0.0064}$	$0.0579^{+0.0069}_{-0.0078}$
H_0	68.45 ± 0.34	$68.79^{+0.35}_{-0.40}$
n_s	0.9685 ± 0.0034	0.9705 ± 0.0034
σ_8	$0.8073^{+0.0048}_{-0.0056}$	0.8120 ± 0.0074
α	$0.25^{+0.09}_{-0.20}$	$0.73^{+0.11}_{-0.27}$
β	$0.0095^{+0.0030}_{-0.0087}$	$0.0206^{+0.0076}_{-0.0100}$
$\chi^2_{min,\rm CDE} - \chi^2_{min,\Lambda}$	-0.90	-1.34
$\ln B_{\rm CDE,\Lambda}$	-7.83	-7.95
Parameter	P18lens+SH0ES+H0LICOW	-
$\Omega_{dm}^{(0)}h^2$	$0.1182^{+0.0011}_{-0.0010}$	-
$\Omega_b^{(0)}h^2$	$0.02259^{+0.00014}_{-0.00016}$	-
τ	$0.0637^{+0.0065}_{-0.0096}$	-
H_0	68.99 ± 0.51	-
n_s	0.9713 ± 0.0037	-
σ_8	0.8160 ± 0.0068	-
α	$0.33^{+0.19}_{-0.23}$	-
β	$0.0197^{+0.0094}_{-0.0084}$	-
$\chi^2_{min,\rm CDE} - \chi^2_{min,\Lambda}$	-1.46	-
$\ln B_{\rm CDE,\Lambda}$	-8.75	-

- Redshift-spcae distortions (RSD): We also use large-scale structure measurements from the anisotropic clustering of galaxies in redshift space. Galaxy redshift surveys provide constraints on the product of the growth rate of structure, $f(z) = \frac{d \ln \delta_m(a)}{d \ln a}$, and the *rms* of mass fluctuations at scales of $8h^{-1}$ Mpc, $\sigma_8(z)$. The data points employed in this work are found in Refs.[30,71,87–95]. The internal correlations between the BAO and RSD data from[71] and[30] have been duly taken into account through the corresponding covariance matrices provided in these two references.
- SH0ES: In some of our data set combinations we include the prior on the Hubble parameter, $H_{0,\mathrm{SH0ES}} = (74.03 \pm 1.42)$ km/s/Mpc obtained by the SH0ES Team with the cosmic distance ladder method.[15] This value of the Hubble parameter is in 4.4σ tension with the TTTEEE+lowE+lensing best-fit ΛCDM model of *Planck* 2018,[9] $H_0 = 67.36 \pm 0.54$ km/s/Mpc.
- H0LICOW: In combination with the prior on H_0 from SH0ES we also use the angular diameter distances reported by the H0LICOW collaboration. They analyze six gravitationally lensed quasars of variable luminosity. After measuring the time delay between the deflected light rays and modeling the lenses they are able to measure the so-called time-delay distances $D_{\Delta t}$ (cf.[29] and references therein). We use their reported six time-delay distances (one for each lensed system), and one distance to the deflector B1608+656, which according to the authors of[29] is uncorrelated with the corresponding $D_{\Delta t}$. The relevant information for building the likelihood can be found in Tables 1 and 2 of,[29] and their captions. Assuming the concordance model, these distances lead to a value of $H_0 = (73.3^{+1.7}_{-1.8})$ km/s/Mpc, which is in 3.2σ tension with the one obtained from the TTTEEE+lowE+lensing analysis by *Planck*.[9]

For more detailed information about these data sets see Ref.[1] and the original observational works.

We proceed now to describe the data set combinations under which we have obtained the main results of this work. They are discussed in detail in Sec. 4. We put constraints using the following combinations: (i) TTTEEE+lowE CMB data from *Planck* 2018,[9] in order to see the constraining power of the CMB when used alone, and also to check whether these data lead to a higher value of H_0 than in the ΛCDM. For simplicity, we will refer to this data set as P18 throughout the paper; (ii) P18+BSC, with BSC denoting the background data set BAO+SNIa+CCH; (iii) We add on top of the latter the linear structure formation information contained in the RSD data, P18+BSC+RSD; (iv) We study the impact of the CMB lensing by also adding the corresponding likelihood, P18lens+BSC+RSD; (v) Finally, we analyze the impact of the prior on H_0 from SH0ES[15] and the H0LICOW angular diameter distances[29] by using the data sets P18+SH0ES+H0LICOW, P18lens+SH0ES+H0LICOW and P18+BSC+SH0ES+H0LICOW. The distance ladder and strong-lensing time delay measurements of the Hubble constant are

completely independent (see e.g. the reviews[96,97]). When combined, they lead to

$$H_{0,comb} = (73.74 \pm 1.10)\,\mathrm{km/s/Mpc}\,, \tag{7}$$

in 5.2σ tension with the best-fit ΛCDM value reported by *Planck* 2018.[9] Hence, it is interesting to check what is the response of the CDE model under these concrete data sets, and to compare the results with those obtained using only the CMB likelihood.

4. Results

Our main results are presented in Table 1 and Figs. 3-4. When we only employ the CMB temperature and polarization data from *Planck* 2018[9] (i.e. the P18 data set) to constrain the CDE model, the fitting values obtained for α and β are compatible at 1σ c.l. with 0, i.e. with a cosmological constant and no interaction in the dark sector (cf. the first row, first column in Table 1). The value of H_0 remains low, roughly 4.1σ below the cosmic distance ladder measurement of.[15] Similarly, when we combine *Planck* with BSC background data or with BSC+RSD, we get a value of H_0 which is 3.8σ and 3.7σ away from the SH0ES value, respectively.

As we have explained in Sec. 2, there is a degeneracy between the strength of the fifth force, i.e. the parameter β, and the Hubble parameter. CDE is in principle able to lower the value of the sound horizon at the decoupling time, r_s, and the amplitude of the first peak of the $\mathcal{D}_l^{TT}$'s. The CMB data fix with high precision the angle $\theta_* = r_s/D_A^{(c)}(z_{dec})$, with $D_A^{(c)}(z_{dec})$ the comoving angular diameter distance to the CMB last scattering surface. This means that in order to keep this ratio constant, H_0 will tend to grow for increasing values of the coupling strength, so that $D_A^{(c)}(z_{dec})$ decreases and compensates in this way the lowering of r_s, while keeping the height of the first peak compatible with data. This positive correlation between H_0 and β can be appreciated in the left-most contour plot of Fig. 3. The latter shows 1 and 2σ posterior probabilities for a selection of cosmological parameters. As discussed, we confirm from the first plot a mild degeneracy between H_0 and β. The strength of the fifth force does not seem to be very degenerate with σ_8 nor with the potential parameter α.

The impact of adding background data on top of P18 can be grasped by looking at the one-dimensional posterior distributions of Fig. 3 (in blue), and also at the numbers of the first row/second column of Table 1. Using the P18+BSC combined data set we find that β and α are now ~ 2.5 and $\sim 3.1\sigma$ away from 0, respectively. The values of H_0 and σ_8, are however compatible at 1σ with the ones obtained using only the P18 data set. They are also fully compatible with those obtained with the ΛCDM under the same data set, which read: $H_0 = (68.29 \pm 0.37)$ km/s/Mpc, $\sigma_8 = 0.812^{+0.006}_{-0.008}$. The peaks in β and α may indicate a mild preference of low-redshift data, when combined with the CMB, for a non-null interaction in the dark sector and a running quintessence potential. As noted already in,[28] we remark that this preference does not seem to correspond to a large improvement in the minimum

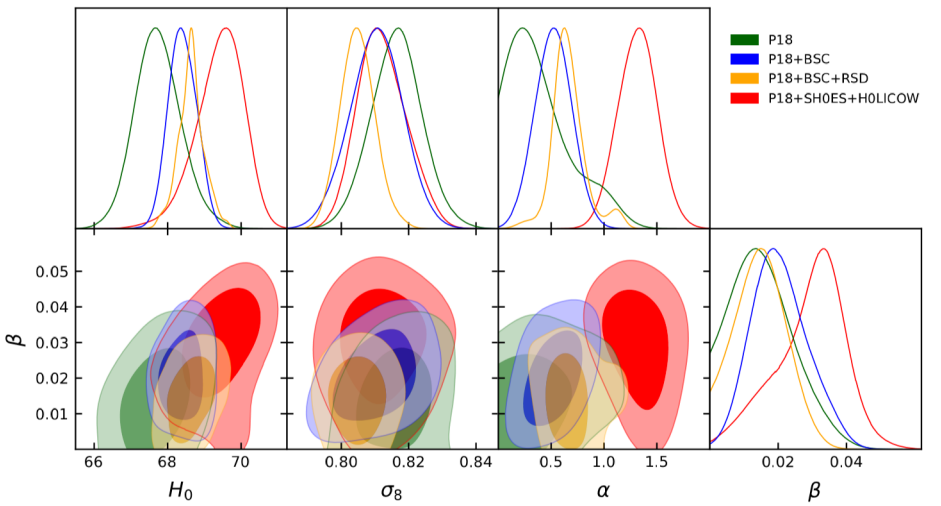

Fig. 3. 1 and 2σ confidence contours obtained using some of the combined data sets described in Sec. 3 in the (H_0, β), (σ_8, β), and (α, β) planes, together with the marginalized one-dimensional posterior distributions for these parameters. See the discussion of these results in Sec. 4.

value of χ^2 with respect to the ΛCDM: under the P18+BSC data set, $\chi^2_{min,\mathrm{CDE}} - \chi^2_{min,\Lambda}$ is negative, but very close to 0, which means that the CDE model only is able to improve the description of the data in a very marginal way.

The addition of the RSD data to the P18+BSC combined data set doesn't change much the result: there is a very small shift in the peak of the one-dimensional posterior distribution for α to larger values and the one for β to lower ones (see the yellow curves in Fig. 3). These two facts reduce a little bit the value of σ_8. The aforesaid peaks are now ~ 5 and $\sim 2\sigma$ away from 0, respectively, with a reduction of χ^2_{min} *w.r.t.* the ΛCDM of 1.56 units (cf. Table 1, second row/second column), i.e. pointing to a very small preference for CDE. The value of H_0 is almost unchanged.

We find important to highlight the specific impact of CMB lensing data with respect to the P18+BSC+RSD data set. If we include also the CMB lensing information, i.e. if we consider the P18lens+BSC+RSD combined data set, posterior probabilities squeeze, as expected, towards the ΛCDM values. This can be seen in Fig. 4, and also in the third row/first column of Table 1.

In order to further evaluate the level at which the degeneracy observed in the (H_0,β)-plane can alleviate the tension in the Hubble parameter between *Planck* and {SH0ES, H0LICOW} data, we perform a Monte Carlo analysis combining those data within the CDE model: results are shown in the second row/first column in Table 1 and correspond to red contours in Fig. 3. In this case, the best fit corresponds to a value of $\beta = 0.0294^{+0.0120}_{-0.0076}$, i.e. at 3σ from zero coupling, a value of $\alpha = 1.32 \pm 0.18$, with $\alpha > 0$ at $\sim 7\sigma$ c.l., and $H_0 = (69.43^{+0.72}_{-0.53})$ km/s/Mpc. The raise of H_0 is

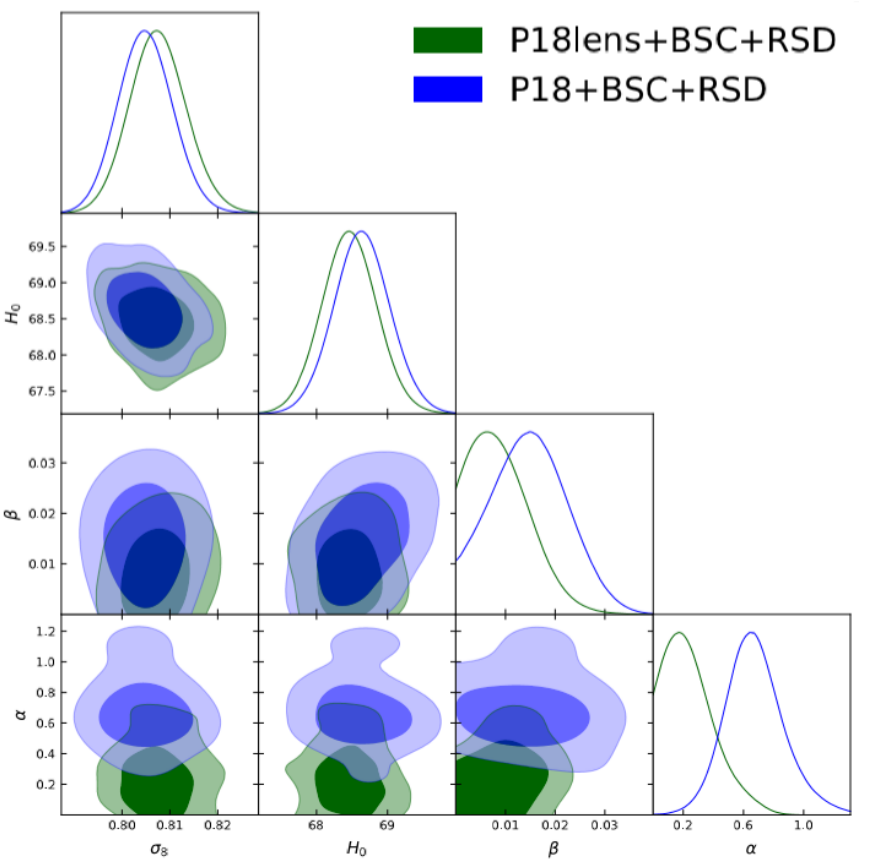

Fig. 4. 1 and 2σ confidence contours obtained with the P18+BSC+RSD and P18lens+BSC+RSD data sets in the most relevant two-dimensional planes of the CDE model parameter space. They allow us to see what is the impact of the CMB lensing on our results. We also show the corresponding marginalized one-dimensional posterior distributions for all the parameters. See the related comments in Sec. 4.

possible thanks to the increase of β, which in turn needs also larger values of α. The tension with the SH0ES+H0LICOW measurement (7) is slightly reduced from 4.8σ (when only P18 is used to constrain the model, cf. the first row/first column of Table 1) to 3.5σ (when also the SH0ES+H0LICOW data are considered). This shifts the H_0 value 1.9σ higher than the best fit using the P18 data set alone, within CDE. Combining also with background data, such as BSC, can partially break degeneracies and leads to $\alpha = 0.73^{+0.11}_{-0.27}$, with $\alpha > 0$ at 3.8σ and $H_0 = (68.79^{+0.35}_{-0.40})$ km/s/Mpc at 4.3σ from the SH0ES+H0LICOW value (7), reducing the chance of CDE to alleviate the tension, as shown in the third row/second column of the table. Finally, the impact of adding CMB lensing is shown in the last row, where now $\beta = 0.0197^{+0.0094}_{-0.0084}$ and $\alpha = 0.33^{+0.19}_{-0.23}$, with $\beta > 0$ and $\alpha > 0$ at 2.2σ and 1.6σ,

respectively, i.e. shifting back towards ΛCDM. In this case $H_0 = (68.99 \pm 0.51)$ km/s/Mpc, 3.9σ away from the SH0ES+H0LICOW value (7) and even more had we included also BSC.

Finally, we can further quantify the relative ability of the CDE model to describe the various data sets *w.r.t.* the ΛCDM cosmology using the Bayes ratio, in alternative to the more approximate χ^2 estimate we mentioned so far. Given a data set $\mathcal{D}$, the probability of a certain model M_i to be the best one among a given set of models $\{M\}$ reads,

$$P(M_i|\mathcal{D}) = \frac{P(M_i)\mathcal{E}(\mathcal{D}|M_i)}{P(\mathcal{D})}\,, \tag{8}$$

where $P(M_i)$ is the prior probability of the model M_i and $P(\mathcal{D})$ the probability of having the data set $\mathcal{D}$. Obviously, the normalization condition $\sum_{j\in\{M\}} P(M_j) = 1$ must be fulfilled. The quantity $\mathcal{E}(\mathcal{D}|M_i)$ is the so-called marginal likelihood or evidence. If the model M_i has n parameters $p_1^{M_i}, p_2^{M_i}, ..., p_n^{M_i}$, the evidence takes the following form,

$$\mathcal{E}(\mathcal{D}|M_i) = \int \mathcal{L}(\mathcal{D}|\vec{p}^{M_i}, M_i)\pi(\vec{p}^{M_i})d^n p^{M_i}\,, \tag{9}$$

with $\mathcal{L}(\mathcal{D}|\vec{p}^{M_i}, M_i)$ being the likelihood and $\pi(\vec{p}^{M_i})$ the prior of the parameters entering the model M_i. The evidence is larger for those models that have more overlapping volume between the likelihood and the prior distributions, but penalizes the use of additional parameters having a non-null impact on the likelihood. Hence, the evidence constitutes a good way of quantifying the performance of the model by implementing in practice the Occam razor principle. If we compare the CDE and ΛCDM models by assuming equal prior probability for both of them, i.e. $P(\text{CDE}) = P(\Lambda\text{CDM})$, then we find that the ratio of their associated probabilities is directly given by the ratio of their corresponding evidences, i.e.

$$\frac{P(\text{CDE}|\mathcal{D})}{P(\Lambda\text{CDM}|\mathcal{D})} = \frac{\mathcal{E}(\mathcal{D}|\text{CDE})}{\mathcal{E}(\mathcal{D}|\Lambda\text{CDM})} \equiv B_{\text{CDE},\Lambda}\,. \tag{10}$$

This is known as Bayes ratio and is the quantity we are interested in. For more details we refer the reader to.[18,98,99] Notice that the computation of (10) is not an easy task in general, since we usually work with models with a high number of (mostly nuisance) parameters, so the integrals under consideration becomes quite involved. We have computed the evidences numerically using the Markov chains obtained from the Monte Carlo analyses and with the aid of the numerical code `MCEvidence`,[68] which is publicly available (cf. Sec. 3). We report the values obtained for the natural logarithm of the Bayes ratio (10) in the last row of Table 1. For all the data sets under study we find values of $\ln(B_{\text{CDE},\Lambda}) < -5$, which point to a preference of the ΛCDM over the CDE model according to Jeffreys' scale.[18,98,99] Although the CDE model we are studying here is able to reduce slightly the value of χ^2_{min} *w.r.t.* the ΛCDM, it has two additional parameters, namely α and β. Moreover, the initial value of the scalar field, ϕ_{ini}, is also left free in the Monte Carlo analysis,

cf. Appendix A of Ref.[1] for details[b]. It turns out that the decrease in χ^2_{min} is insufficient to compensate the penalization introduced by the use of these extra parameters. If instead of using the evidences (9) and the Bayes ratio (10) to perform the model comparison we make use of e.g. the Akaike,[100] Bayesian[101] or Deviance[102] information criteria, we reach similar conclusions[c]. We want to note, though, that all these information criteria are approximations of the exact Bayesian approach. Although they allow to skip the demanding computation of the evidence (9), they are only reliable when the posterior distribution is close to a multivariate Gaussian (which is not the case under study), and the Akaike and Bayesian criteria do not take into account the impact of priors nor the existing correlations between the parameters.

Similar results and conclusions are reached using an exponential potential for the scalar field, instead of (6). See appendix C of Ref.[1].

Finally, it is worth to mention that our results are compatible with the ones obtained in the context of the Ricci running vacuum models (RVMs) of type I recently studied in Ref.[48], in which there is also an interaction in the dark sector between dark matter and a dynamical vacuum component with $p_{\rm vac} = -\rho_{\rm vac}$ and $\rho_{\rm vac}(\mathcal{R}) = \frac{3}{8\pi G_N}\left(c_0 + \frac{\nu}{12}\mathcal{R}\right)$, where $\mathcal{R} = 12H^2 + 6\dot{H}$ is the Ricci scalar. These models can be motivated using renormalization group arguments in QFT in curved space-time, see Refs.[12,103] and references therein. In Ref.[48] the authors show that these RVMs are also unable to alleviate the cosmological tensions significantly when the interaction is active around the CMB decoupling time. Allowing for a late-time activation of the interaction around $z \sim 1$, with an energy transfer from the vacuum to the matter sectors, it is possible to mitigate the σ_8 tension due to the increase of the relative amount of vacuum energy with respect to dark matter in the past. Nevertheless, the H_0 tension persists. Other Ricci RVMs (those of Type II) are able to soften both tensions at a time, see[48] for further details.

5. Conclusions

Cosmological observations help to test the dark sector, and in particular interactions between dark matter particles, mediated by a dark energy scalar field, as in CDE cosmologies. Up to a conformal transformation, this is another way of testing gravity at large scales. In this paper we carried out this task in one of the simplest and most studied models, namely, a dark energy-dark matter conformal coupling with a

[b]In the computation of the evidence (9) for the CDE model we have employed the following flat priors for the extra parameters: $0 < \beta < 0.1$, $0 < \alpha < 2$, and $0 < \kappa\phi_{ini} < 50$. Slightly broader or tighter priors can be considered, but $\ln(B_{\rm CDE,\Lambda})$ only changes logarithmically, so our conclusions are not very sensitive to them.

[c]For instance, Akaike criterion[100] is given by $\mathrm{AIC} = \chi^2_{min} + 2n$, where n is the number of parameters in the model (the degree of correlation between them is not taken into account). Considering that CDE with PR potential has an effective number of parameters between 2 and 3 we find $2.5 < \mathrm{AIC}_{\rm CDE} - \mathrm{AIC}_\Lambda < 6$ for the scenarios explored in Table 1, which leads to a positive preference for ΛCDM, again using Jeffreys' scale.[18,98,99]

Peebles-Ratra potential. CDE might probe helpful to explain the well-known tension between local and cosmological values of H_0. Any detection of a varying dark energy potential or interaction would clearly constitute a major result and it is therefore important to monitor the constraints that newer data impose. This is particularly true in view of earlier results that detected a non-zero value of the coupling β.[27,28]

We confirm the existence of a peak in the marginalized posterior distribution for β and α, more or less evident depending on the data set combination. While for P18 + SH0ES + H0LICOW $\beta > 0$ at 3σ and $\alpha > 0$ at nearly 7σ, inclusion of background data reduces the evidence to $\beta > 0$ at 2.3σ and $\alpha > 0$ at nearly 3.8σ. Inclusion of CMB lensing shifts both values to be compatible with ΛCDM within 2σ. We find it important to stress that specifically CMB lensing prefers ΛCDM. In all cases, we find that, overall, the peak does not correspond to a better Bayes ratio and ΛCDM remains the favored model when employing Bayesian model comparison, given the extra parameters introduced within the model. With regard to H_0, we find that under the P18+SH0ES+H0LICOW combined data set the simple coupled model with constant coupling investigated in this work leads to a value in 3.5σ tension with (7), or in 4.3σ tension when including further background data. The values of σ_8 are also similar to those found in the ΛCDM (i.e. $\sigma_8 \sim 0.80 - 0.82$), even when RSD data are considered together with CMB and background data. In this case we find $\beta = 0.010^{+0.003}_{-0.009}$ and $\beta = 0.015^{+0.007}_{-0.008}$, with and without CMB lensing, respectively. For the values of the coupling strength preferred by the data we find the typical increase of the mass of the DM particles to be $m(\phi_{ini})/m^{(0)} - 1 \lesssim \mathcal{O}(1)\%$.

The question that naturally arises is then, which modification of CDE can help alleviating the tensions? One can immediately suppose that a varying β can go some way towards this. Or, it could be that a model with both energy- and momentum-couplings (see e.g.[104]), which can introduce a weaker gravity, helps with the tensions. These issues will be investigated in future publications.

Acknowledgments

I want to express my most sincere gratitude to Prof. Mavromatos for his invitation to give my talk at the very interesting DM1 parallel session of the MG16 Meeting. I also want to thank Prof. Luca Amendola and Valeria Pettorino for their collaboration in the work my presentation of July 5th 2021 was based on, namely arXiv:2004.00610.[1]

References

1. A. Gómez-Valent, V. Pettorino and L. Amendola, Update on coupled dark energy and the H_0 tension, *Phys. Rev. D* **101**, p. 123513 (2020).
2. A. G. Riess *et al.*, Observational evidence from supernovae for an accelerating universe and a cosmological constant, *Astron. J.* **116**, 1009 (1998).
3. S. Perlmutter *et al.*, Measurements of Ω and Λ from 42 high redshift supernovae, *Astrophys. J.* **517**, 565 (1999).
4. S. Cole *et al.*, The 2dF Galaxy Redshift Survey: Power-spectrum analysis of the final dataset and cosmological implications, *Mon. Not. Roy. Astron. Soc.* **362**, 505 (2005).

5. D. J. Eisenstein *et al.*, Detection of the Baryon Acoustic Peak in the Large-Scale Correlation Function of SDSS Luminous Red Galaxies, *Astrophys. J.* **633**, 560 (2005).
6. G. Hinshaw *et al.*, Nine-Year Wilkinson Microwave Anisotropy Probe (WMAP) Observations: Cosmological Parameter Results, *Astrophys. J. Suppl.* **208**, p. 19 (2013).
7. P. A. R. Ade *et al.*, Planck 2013 results. I. Overview of products and scientific results, *Astron. Astrophys.* **571**, p. A1 (2014).
8. P. A. R. Ade *et al.*, Planck 2015 results. XIII. Cosmological parameters, *Astron. Astrophys.* **594**, p. A13 (2016).
9. N. Aghanim *et al.*, Planck 2018 results. VI. Cosmological parameters, *Astron. Astrophys.* **641**, p. A6 (2020), [Erratum: Astron.Astrophys. 652, C4 (2021)].
10. S. Weinberg, The Cosmological Constant Problem, *Rev. Mod. Phys.* **61**, 1 (1989), [,569(1988)].
11. J. Martin, Everything You Always Wanted To Know About The Cosmological Constant Problem (But Were Afraid To Ask), *Comptes Rendus Physique* **13**, 566 (2012).
12. J. Solà, Cosmological constant and vacuum energy: old and new ideas, *J. Phys. Conf. Ser.* **453**, p. 012015 (2013).
13. P. J. E. Peebles and B. Ratra, The Cosmological Constant and Dark Energy, *Rev. Mod. Phys.* **75**, 559 (2003).
14. T. Padmanabhan, Cosmological constant: The Weight of the vacuum, *Phys. Rept.* **380**, 235 (2003).
15. A. G. Riess, S. Casertano, W. Yuan, L. M. Macri and D. Scolnic, Large Magellanic Cloud Cepheid Standards Provide a 1% Foundation for the Determination of the Hubble Constant and Stronger Evidence for Physics beyond ΛCDM, *Astrophys. J.* **876**, p. 85 (2019).
16. E. Macaulay, I. K. Wehus and H. K. Eriksen, Lower Growth Rate from Recent Redshift Space Distortion Measurements than Expected from Planck, *Phys. Rev. Lett.* **111**, p. 161301 (2013).
17. H. Hildebrandt *et al.*, KiDS+VIKING-450: Cosmic shear tomography with optical+infrared data, *Astron. Astrophys.* **633**, p. A69 (2020).
18. L. Amendola and S. Tsujikawa, *Dark Energy: Theory and Observations* (Cambridge Univ. Press, Cambridge, 2015).
19. A. Joyce, B. Jain, J. Khoury and M. Trodden, Beyond the Cosmological Standard Model, *Phys. Rept.* **568**, 1 (2015).
20. C. Wetterich, The Cosmon model for an asymptotically vanishing time dependent cosmological 'constant', *Astron. Astrophys.* **301**, 321 (1995).
21. L. Amendola, Coupled quintessence, *Phys. Rev.* **D62**, p. 043511 (2000).
22. R. D. Peccei, J. Solà and C. Wetterich, Adjusting the Cosmological Constant Dynamically: Cosmons and a New Force Weaker Than Gravity, *Phys. Lett.* **B195**, 183 (1987).
23. C. Wetterich, Cosmology and the Fate of Dilatation Symmetry, *Nucl. Phys.* **B302**, 668 (1988).
24. P. J. E. Peebles and B. Ratra, Cosmology with a Time Variable Cosmological Constant, *Astrophys. J.* **325**, p. L17 (1988).
25. B. Ratra and P. J. E. Peebles, Cosmological Consequences of a Rolling Homogeneous Scalar Field, *Phys. Rev.* **D37**, p. 3406 (1988).
26. V. Pettorino, L. Amendola, C. Baccigalupi and C. Quercellini, Constraints on coupled dark energy using CMB data from WMAP and SPT, *Phys. Rev.* **D86**, p. 103507 (2012).
27. V. Pettorino, Testing modified gravity with Planck: the case of coupled dark energy, *Phys. Rev.* **D88**, p. 063519 (2013).

28. P. A. R. Ade *et al.*, Planck 2015 results. XIV. Dark energy and modified gravity, *Astron. Astrophys.* **594**, p. A14 (2016).
29. K. C. Wong *et al.*, H0LiCOW XIII. A 2.4% measurement of H_0 from lensed quasars: 5.3σ tension between early and late-Universe probes (2019).
30. H. Gil-Marín *et al.*, The clustering of the SDSS-IV extended Baryon Oscillation Spectroscopic Survey DR14 quasar sample: structure growth rate measurement from the anisotropic quasar power spectrum in the redshift range $0.8 < z < 2.2$, *Mon. Not. Roy. Astron. Soc.* **477**, 1604 (2018).
31. J.-Q. Xia, New Limits on Coupled Dark Energy from Planck, *JCAP* **1311**, p. 022 (2013).
32. A. Pourtsidou and T. Tram, Reconciling CMB and structure growth measurements with dark energy interactions, *Phys. Rev.* **D94**, p. 043518 (2016).
33. C. van de Bruck, J. Mifsud and J. Morrice, Testing coupled dark energy models with their cosmological background evolution, *Phys. Rev.* **D95**, p. 043513 (2017).
34. C. van de Bruck and J. Mifsud, Searching for dark matter - dark energy interactions: going beyond the conformal case, *Phys. Rev.* **D97**, p. 023506 (2018).
35. Y.-H. Li, J.-F. Zhang and X. Zhang, Exploring the full parameter space for an interacting dark energy model with recent observations including redshift-space distortions: Application of the parametrized post-Friedmann approach, *Phys. Rev.* **D90**, p. 123007 (2014).
36. Y.-H. Li, J.-F. Zhang and X. Zhang, Testing models of vacuum energy interacting with cold dark matter, *Phys. Rev.* **D93**, p. 023002 (2016).
37. E. Di Valentino, A. Melchiorri and O. Mena, Can interacting dark energy solve the H_0 tension?, *Phys. Rev.* **D96**, p. 043503 (2017).
38. E. G. M. Ferreira, J. Quintin, A. A. Costa, E. Abdalla and B. Wang, Evidence for interacting dark energy from BOSS, *Phys. Rev.* **D95**, p. 043520 (2017).
39. A. A. Costa, X.-D. Xu, B. Wang and E. Abdalla, Constraints on interacting dark energy models from Planck 2015 and redshift-space distortion data, *JCAP* **1701**, p. 028 (2017).
40. J. Solà, A. Gómez-Valent and J. de Cruz Pérez, The H_0 tension in light of vacuum dynamics in the Universe, *Phys. Lett.* **B774**, 317 (2017).
41. J. Solà Peracaula, J. de Cruz Pérez and A. Gómez-Valent, Possible signals of vacuum dynamics in the Universe, *Mon. Not. Roy. Astron. Soc.* **478**, 4357 (2018).
42. M. Martinelli, N. B. Hogg, S. Peirone, M. Bruni and D. Wands, Constraints on the interacting vacuum–geodesic CDM scenario, *Mon. Not. Roy. Astron. Soc.* **488**, 3423 (2019).
43. P. Agrawal, G. Obied and C. Vafa, H_0 tension, swampland conjectures, and the epoch of fading dark matter, *Phys. Rev. D* **103**, p. 043523 (2021).
44. S. Pan, G. S. Sharov and W. Yang, Field theoretic interpretations of interacting dark energy scenarios and recent observations, *Phys. Rev. D* **101**, p. 103533 (2020).
45. J. Solà Peracaula, J. de Cruz Pérez and A. Gómez-Valent, Dynamical dark energy vs. Λ = const in light of observations, *EPL* **121**, p. 39001 (2018).
46. A. Gómez-Valent and J. Solà Peracaula, Density perturbations for running vacuum: a successful approach to structure formation and to the σ_8-tension, *Mon. Not. Roy. Astron. Soc.* **478**, 126 (2018).
47. P. Tsiapi and S. Basilakos, Testing dynamical vacuum models with CMB power spectrum from Planck, *Mon. Not. Roy. Astron. Soc.* **485**, 2505 (2019).
48. J. Solà Peracaula, A. Gómez-Valent, J. de Cruz Perez and C. Moreno-Pulido, Running vacuum against the H_0 and σ_8 tensions, *EPL* **134**, p. 19001 (2021).

49. L. Amendola, Linear and non-linear perturbations in dark energy models, *Phys. Rev.* **D69**, p. 103524 (2004).
50. V. Pettorino and C. Baccigalupi, Coupled and Extended Quintessence: theoretical differences and structure formation, *Phys. Rev.* **D77**, p. 103003 (2008).
51. L. Amendola and V. Pettorino, Beyond self-acceleration: force- and fluid-acceleration, *Phys. Lett.* **B802**, p. 135214 (2020).
52. C. M. Will, The Confrontation between general relativity and experiment, *Living Rev. Rel.* **9**, p. 3 (2006).
53. B. Elder, V. Vardanyan, Y. Akrami, P. Brax, A.-C. Davis and R. S. Decca, The Classical Symmetron Force in Casimir Experiments, *Phys. Rev.* **D101**, p. 064065 (2020).
54. P. Brax, A.-C. Davis, B. Elder and L. K. Wong, Constraining screened fifth forces with the electron magnetic moment, *Phys. Rev.* **D97**, p. 084050 (2018).
55. J. Bergé, P. Brax, G. Métris, M. Pernot-Borràs, P. Touboul and J.-P. Uzan, MICROSCOPE Mission: First Constraints on the Violation of the Weak Equivalence Principle by a Light Scalar Dilaton, *Phys. Rev. Lett.* **120**, p. 141101 (2018).
56. G. Efstathiou and S. Gratton, The evidence for a spatially flat Universe (2020).
57. R. K. Sachs and A. M. Wolfe, Perturbations of a cosmological model and angular variations of the microwave background, *Astrophys. J.* **147**, 73 (1967), [Gen. Rel. Grav.39,1929(2007)].
58. L. Amendola, V. Pettorino, C. Quercellini and A. Vollmer, Testing coupled dark energy with next-generation large-scale observations, *Phys. Rev.* **D85**, p. 103008 (2012).
59. M. Baldi, V. Pettorino, G. Robbers and V. Springel, Hydrodynamical N-body simulations of coupled dark energy cosmologies, *Mon. Not. Roy. Astron. Soc.* **403**, 1684 (2010).
60. M. Baldi and V. Pettorino, High-z massive clusters as a test for dynamical coupled dark energy, *Mon. Not. Roy. Astron. Soc.* **412**, p. L1 (2011).
61. L. Amendola and C. Quercellini, Tracking and coupled dark energy as seen by WMAP, *Phys. Rev.* **D68**, p. 023514 (2003).
62. J. Solà, A. Gómez-Valent and J. de Cruz Pérez, Dynamical dark energy: scalar fields and running vacuum, *Mod. Phys. Lett.* **A32**, p. 1750054 (2017).
63. J. Ooba, B. Ratra and N. Sugiyama, Planck 2015 constraints on spatially-flat dynamical dark energy models, *Astrophys. Space Sci.* **364**, p. 176 (2019).
64. J. Solà Peracaula, A. Gómez-Valent and J. de Cruz Pérez, Signs of Dynamical Dark Energy in Current Observations, *Phys. Dark Univ.* **25**, p. 100311 (2019).
65. D. Blas, J. Lesgourgues and T. Tram, The Cosmic Linear Anisotropy Solving System (CLASS) II: Approximation schemes, *JCAP* **1107**, p. 034 (2011).
66. B. Audren, J. Lesgourgues, K. Benabed and S. Prunet, Conservative Constraints on Early Cosmology: an illustration of the Monte Python cosmological parameter inference code, *JCAP* **1302**, p. 001 (2013).
67. A. Lewis, GetDist: a Python package for analysing Monte Carlo samples (2019).
68. A. Heavens, Y. Fantaye, A. Mootoovaloo, H. Eggers, Z. Hosenie, S. Kroon and E. Sellentin, Marginal Likelihoods from Monte Carlo Markov Chains (2017).
69. N. Aghanim *et al.*, Planck 2018 results. VIII. Gravitational lensing, *Astron. Astrophys.* **641**, p. A8 (2020).
70. P. Carter, F. Beutler, W. J. Percival, C. Blake, J. Koda and A. J. Ross, Low Redshift Baryon Acoustic Oscillation Measurement from the Reconstructed 6-degree Field Galaxy Survey, *Mon. Not. Roy. Astron. Soc.* **481**, 2371 (2018).

71. H. Gil-Marín, W. J. Percival, L. Verde, J. R. Brownstein, C.-H. Chuang, F.-S. Kitaura, S. A. Rodríguez-Torres and M. D. Olmstead, The clustering of galaxies in the SDSS-III Baryon Oscillation Spectroscopic Survey: RSD measurement from the power spectrum and bispectrum of the DR12 BOSS galaxies, *Mon. Not. Roy. Astron. Soc.* **465**, 1757 (2017).
72. E. A. Kazin *et al.*, The WiggleZ Dark Energy Survey: improved distance measurements to z = 1 with reconstruction of the baryonic acoustic feature, *Mon. Not. Roy. Astron. Soc.* **441**, 3524 (2014).
73. T. M. C. Abbott *et al.*, Dark Energy Survey Year 1 Results: Measurement of the Baryon Acoustic Oscillation scale in the distribution of galaxies to redshift 1, *Mon. Not. Roy. Astron. Soc.* **483**, 4866 (2019).
74. M. Blomqvist *et al.*, Baryon acoustic oscillations from the cross-correlation of Lyα absorption and quasars in eBOSS DR14, *Astron. Astrophys.* **629**, p. A86 (2019).
75. V. de Sainte Agathe *et al.*, Baryon acoustic oscillations at z = 2.34 from the correlations of Lyα absorption in eBOSS DR14, *Astron. Astrophys.* **629**, p. A85 (2019).
76. D. M. Scolnic *et al.*, The Complete Light-curve Sample of Spectroscopically Confirmed SNe Ia from Pan-STARRS1 and Cosmological Constraints from the Combined Pantheon Sample, *Astrophys. J.* **859**, p. 101 (2018).
77. A. G. Riess *et al.*, Type Ia Supernova Distances at Redshift > 1.5 from the Hubble Space Telescope Multi-cycle Treasury Programs: The Early Expansion Rate, *Astrophys. J.* **853**, p. 126 (2018).
78. R. Jiménez, L. Verde, T. Treu and D. Stern, Constraints on the equation of state of dark energy and the Hubble constant from stellar ages and the CMB, *Astrophys. J.* **593**, 622 (2003).
79. J. Simon, L. Verde and R. Jiménez, Constraints on the redshift dependence of the dark energy potential, *Phys. Rev.* **D71**, p. 123001 (2005).
80. D. Stern, R. Jiménez, L. Verde, M. Kamionkowski and S. A. Stanford, Cosmic Chronometers: Constraining the Equation of State of Dark Energy. I: H(z) Measurements, *JCAP* **1002**, p. 008 (2010).
81. M. Moresco *et al.*, Improved constraints on the expansion rate of the Universe up to z 1.1 from the spectroscopic evolution of cosmic chronometers, *JCAP* **1208**, p. 006 (2012).
82. C. Zhang, H. Zhang, S. Yuan, T.-J. Zhang and Y.-C. Sun, Four new observational $H(z)$ data from luminous red galaxies in the Sloan Digital Sky Survey data release seven, *Res. Astron. Astrophys.* **14**, 1221 (2014).
83. M. Moresco, Raising the bar: new constraints on the Hubble parameter with cosmic chronometers at $z \sim 2$, *Mon. Not. Roy. Astron. Soc.* **450**, L16 (2015).
84. M. Moresco, L. Pozzetti, A. Cimatti, R. Jiménez, C. Maraston, L. Verde, D. Thomas, A. Citro, R. Tojeiro and D. Wilkinson, A 6% measurement of the Hubble parameter at $z \sim 0.45$: direct evidence of the epoch of cosmic re-acceleration, *JCAP* **1605**, p. 014 (2016).
85. A. L. Ratsimbazafy, S. I. Loubser, S. M. Crawford, C. M. Cress, B. A. Bassett, R. C. Nichol and P. Väisänen, Age-dating Luminous Red Galaxies observed with the Southern African Large Telescope, *Mon. Not. Roy. Astron. Soc.* **467**, 3239 (2017).
86. A. Gómez-Valent, Quantifying the evidence for the current speed-up of the Universe with low and intermediate-redshift data. A more model-independent approach, *JCAP* **1905**, p. 026 (2019).
87. F. Qin, C. Howlett and L. Staveley-Smith, The redshift-space momentum power spectrum — II. Measuring the growth rate from the combined 2MTF and 6dFGSv surveys, *Mon. Not. Roy. Astron. Soc.* **487**, 5235 (2019).

88. F. Shi *et al.*, Mapping the Real Space Distributions of Galaxies in SDSS DR7: II. Measuring the growth rate, clustering amplitude of matter and biases of galaxies at redshift 0.1, *Astrophys. J.* **861**, p. 137 (2018).
89. F. Simpson, C. Blake, J. A. Peacock, I. Baldry, J. Bland-Hawthorn, A. Heavens, C. Heymans, J. Loveday and P. Norberg, Galaxy and mass assembly: Redshift space distortions from the clipped galaxy field, *Phys. Rev.* **D93**, p. 023525 (2016).
90. C. Blake *et al.*, Galaxy And Mass Assembly (GAMA): improved cosmic growth measurements using multiple tracers of large-scale structure, *Mon. Not. Roy. Astron. Soc.* **436**, p. 3089 (2013).
91. C. Blake *et al.*, The WiggleZ Dark Energy Survey: the growth rate of cosmic structure since redshift z=0.9, *Mon. Not. Roy. Astron. Soc.* **415**, p. 2876 (2011).
92. F. G. Mohammad *et al.*, The VIMOS Public Extragalactic Redshift Survey (VIPERS): Unbiased clustering estimate with VIPERS slit assignment, *Astron. Astrophys.* **619**, p. A17 (2018).
93. L. Guzzo *et al.*, A test of the nature of cosmic acceleration using galaxy redshift distortions, *Nature* **451**, 541 (2008).
94. Y.-S. Song and W. J. Percival, Reconstructing the history of structure formation using Redshift Distortions, *JCAP* **0910**, p. 004 (2009).
95. T. Okumura *et al.*, The Subaru FMOS galaxy redshift survey (FastSound). IV. New constraint on gravity theory from redshift space distortions at $z \sim 1.4$, *Publ. Astron. Soc. Jap.* **68**, p. 38 (2016).
96. L. Verde, T. Treu and A. G. Riess, Tensions between the early and late Universe, *Nature Astronomy* **3**, 891 (2019).
97. A. G. Riess, The Expansion of the Universe is Faster than Expected, *Nature Rev. Phys.* **2**, 10 (2020).
98. R. E. Kass and A. E. Raftery, The WiggleZ Dark Energy Survey: improved distance measurements to z = 1 with reconstruction of the baryonic acoustic feature, *J. Amer. Statist. Assoc.* **90**, 773 (1995).
99. K. P. Burnham and D. R. Anderson, *Model selection and multimodel inference* (Springer, New York, 2002).
100. H. Akaike, A new look at the statistical model identification, *IEEE Trans. Autom. Control* **19**, 716 (1974).
101. G. Schwarz, Estimating the Dimension of a Model, *Ann. Stat.* **6**, 461 (1978).
102. D. J. Spiegelhalter, N. G. Best, B. P. Carlin and A. van der Linde, Bayesian measures of model complexity and fit, *J. Roy. Stat. Soc.* **64**, p. 583 (2002).
103. C. Moreno-Pulido and J. Solà Peracaula, Running vacuum in quantum field theory in curved spacetime: renormalizing ρ_{vac} without $\sim m^4$ terms, *Eur. Phys. J. C* **80**, p. 692 (2020).
104. L. Amendola and S. Tsujikawa, Scaling solutions and weak gravity in dark energy with energy and momentum couplings, *JCAP* **06**, p. 020 (2020).